Comparison of M-Side Electron Transfer in *Rb. sphaeroides* and *Rb. capsulatus* Reaction Centers

Christine Kirmaier,[†] Philip D. Laible,[‡] Kazimierz Czarnecki,[§] Aaron N. Hata,[‡] Deborah K. Hanson,*[,‡] David F. Bocian,*[,§] and Dewey Holten*[,†]

Department of Chemistry, Washington University, St. Louis, Missouri 63130-4899, Biosciences Division, Argonne National Laboratory, Argonne, Illinois 60439-4833, and Department of Chemistry, University of California, Riverside, California 92521-0403

Received: August 24, 2001; In Final Form: November 26, 2001

Subpicosecond time-resolved absorption and steady-state resonance Raman studies are reported for *Rhodobacter sphaeroides* reaction centers (RCs) that incorporate the G(M203)D/L(M214)H double mutation (denoted DH). Upon excitation, P* decays with a time constant of 15 ps via a combination of electron transfer to the L side (83%), decay to the ground state (10%), and electron transfer to the M side to form $P^+BPh_M^-$ (7%). On the L-side, branching between charge recombination versus charge separation at the transient intermediate reduces the subsequent $P^+Q_A^-$ yield to 68%. These results differ in detail from those found previously for the *Rb. capsulatus* G(M201)D/L(M212)H analogue (also denoted DH), most notably in a 2-fold lower yield of M-side charge separation in *Rb. sphaeroides*. Studies on the DH mutant in a carotenoidless *Rb. capsulatus* strain give the same spectral signatures and M-side yield found previously in the carotenoid-containing mutant. This finding eliminates any possibility that the Q_X bleaching assigned to reduction of BPh_M is compromised by carotenoid bandshifts resulting simply from L-side charge separation. The collective results reveal significant differences between the rates of charge separation to M side (as well as to the L side) in *Rb. capsulatus* and *Rb. sphaeroides*, which must arise in some or large measure from small differences (perhaps tens of meV) in the free energies of the states in the two species. The relative free energies in turn must derive from differences in the cofactor-protein interactions (in both wild type and mutants), some of which are indicated by resonance Raman data. The differences between the two species have insignificant (though observable) effects on the primary events in wild-type RCs, but have greater consequences when the modest free energy gaps between the states are further reduced in mutants. *Rb. sphaeroides* RCs may in general have a lower propensity for electron transfer to the normally inactive branch, compared to *Rb. capsulatus*.

Introduction

The bacterial reaction center (RC) is a membrane-bound pigment-protein complex that has a macroscopic C_2 symmetric arrangement of the L and M polypeptides and the associated bacteriochlorophyll (BChl), bacteriopheophytin (BPh), and quinone (Q) cofactors.[1] Excitation of the primary electron donor (P, a dimer of BChls) to its lowest excited singlet state (P*), elicits electron transfer exclusively down the L-side of the native pigment-protein complex. Utilizing $BChl_L$ in parallel mechanisms as a discrete or virtual electron carrier, an electron from P* arrives on BPh_L in ∼3 ps, followed by electron transfer to Q_A in ∼200 ps, with an overall quantum yield of ∼1.[2] The same photochemistry, but with differences in rate constants, is observed in wild-type RCs from a variety of purple bacterial species, including *Rb. capsulatus* and *Rb. sphaeroides* (Figure 1).

One approach to probing the mechanisms underlying the directionality and high quantum yield of charge separation has been to use site-directed mutations near the cofactors to modulate the relative free energies of the states.[3−13] Significant effects on the charge separation and recombination events have been observed due to the modest free energy gaps operative in the native RC, which lead to even smaller spacings or reversed orderings of states in many mutants. A working model for the L side in the wild-type RC has $P^+BChl_L^-$ and $P^+BPh_L^-$ very close in free energy, with the former below P* by 0.05−0.1 eV[7,11c,13b,c,14b,d,15c] and the latter (when relaxed) by ∼0.25 eV.[10b,15] The free energy span is reduced when BPh_L is replaced by a BChl molecule (denoted β) as a result of incorporation of a His residue at analogous positions in the *Rb. sphaeroides* RC

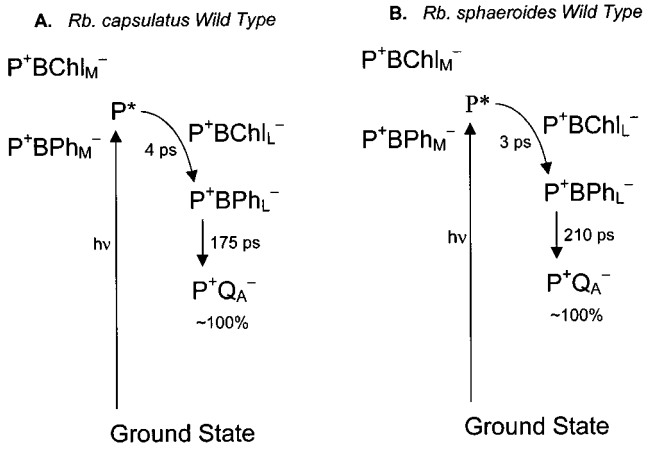

Figure 1. Schematic energy level diagrams for wild-type RCs from (a) *Rb. capsulatus* and (b) *Rb. sphaeroides*.

[†] Department of Chemistry, Washington University.
[‡] Biosciences Division, Argonne National Laboratory.
[§] Department of Chemistry, University of California, Riverside.

10.1021/jp013264w CCC: $22.00
Published on Web 01/30/2002

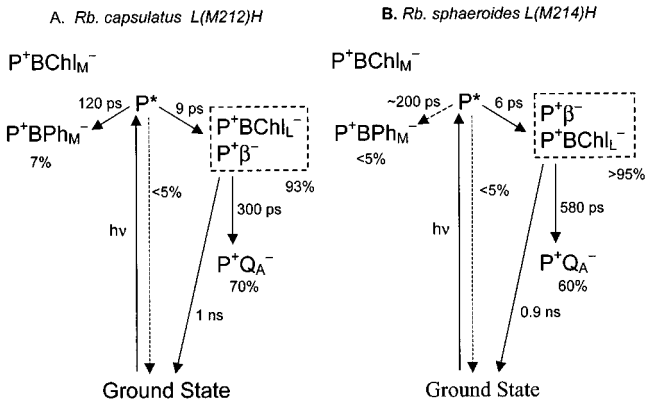

Figure 2. Schematic energy level diagrams for the H mutants: (a) *Rb. capsulatus* L(M212)H and (b) *Rb. sphaeroides* L(M214)H. The dashed box indicates that states $P^+\beta^-$ and $P^+BChl_L^-$ are so close that quantum/thermal mixing between them occurs (giving an intermediate generically termed P^+I^-). It appears that $P^+BChl_L^-$ lies slightly below $P^+\beta^-$ in the *Rb. sphaeroides* mutant and that the two states are essentially degenerate in the *Rb. capsulatus* analogue.[3b,9b,11c]

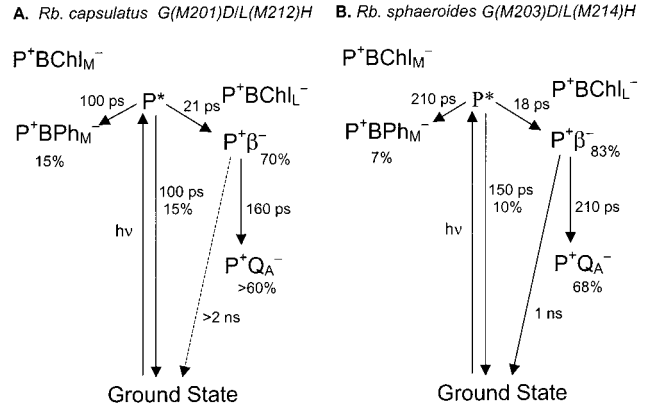

Figure 3. Schematic energy level diagrams for the DH mutants: (a) *Rb. capsulatus* G(M201)D/L(M212)H and (b) *Rb. sphaeroides* G(M203)D/L(M214)H.

[L(M214)H] and the *Rb. capsulatus* RC [L(M212)H]; these mutants are denoted H.[9] State $P^+\beta^-$ is sufficiently close to $P^+BChl_L^-$ that quantum/thermal mixing between them (giving an intermediate generically termed P^+I^-) causes enhanced charge recombination to give the ground state and diminished charge separation to form $P^+Q_A^-$ (Figure 2).[16] Indeed, the states are so close that very small differences in the protein-cofactor interactions in *Rb. sphaeroides* versus *Rb. capsulatus* RCs apparently result in different spacing/ordering of $P^+\beta^-$ and $P^+BChl_L^-$ and thus, altered L-side charge separation/recombination ratios and consequent $P^+Q_A^-$ yields in the two species.[11c]

Photoinduced electron transfer down the M-branch to form $P^+BPh_M^-$ was first observed when a second mutation was added to the L(M212)H template in *Rb. capsulatus* to produce the G(M201)D/L(M212)H double mutant (denoted DH).[11a] The G(M201)D mutation places an Asp near ring V of $BChl_L$, raising $P^+BChl_L^-$ significantly in free energy so as to place this state well above $P^+\beta^-$ and perhaps slightly above P* (Figure 3A).[17] The resulting slower electron transfer to the L side allows for competing electron transfer to BPh_M to occur in 15% yield at room temperature. The interactions between Asp M201 and $BChl_L$ that destabilize $P^+BChl_L^-$ have been probed by resonance Raman (RR) spectroscopy.[18]

Given the differences noted above in the L-side events in *Rb. sphaeroides* and *Rb. capsulatus* H mutants—L(M214)H and L(M212)H, respectively—we wondered whether there might be different yields of electron transfer to the M side in the corresponding DH RCs, G(M203)D/L(M214)H and G(M201)D/L(M212)H, respectively.[19] To this end, we have prepared the *Rb. sphaeroides* DH mutant and studied the primary events using subpicosecond resolution transient absorption (TA) techniques, and examined the interactions between Asp M203 and $BChl_L$ via RR spectroscopy. To eliminate the possibility that the BPh_M Q_X absorbance bleaching (used as a key signature of $P^+BPh_M^-$ formation) might be compromised to a degree by a carotenoid band shift derived simply from charge separation down the L branch, we have also studied the primary events in the DH mutant prepared in a carotenoidless *Rb. capsulatus* strain. Collectively, these results give further support for M-side charge separation in modified RCs and reveal differences between species that likely derive from small differences in modest free-energy gaps.

Materials and Methods

Mutagenesis. The construction of the M201Asp-M212His (DH) mutant of *Rb. capsulatus* has been previously described.[11a] We recently incorporated a poly-histidine tag into the 3′-end of the gene encoding the M subunit of *Rb. capsulatus* (P. D. Laible and D. K. Hanson, in preparation); this C-terminal extension facilitates rapid and efficient recovery of RCs of exceptional purity using immobilized metal affinity chromatography (IMAC) protocols.[20b] The preexisting DH mutation was subcloned into the His-tagged expression plasmid using unique KpnI and BamHI restriction sites that flank the M gene in this system. For isolation of carotenoidless *Rb. capsulatus* DH mutant RCs, the mutant plasmid was transferred via conjugation to a carotenoidless (U43B[21d], gift of E. Bylina) strain of *Rb. capsulatus*, complementing deletions of genes for RC and LHI complexes *in trans* as previously described.[21c,22] The *Rb. capsulatus* mutant strains were routinely grown under chemoheterotrophic conditions (semi-aerobic, dark, 34 °C) on a medium designated ^{Super}RCVPY containing kanamycin (30 μg/mL), in the absence of selection for RC function. ^{Super}RCVPY is essentially the medium RCVPY[20c] to which an additional 0.25 g of $(NH_4)_2SO_4$, and 0.75 g each of yeast extract and peptone are added per liter.

The *Rb. sphaeroides* DH mutant was constructed using a system that was previously developed (D. K. Hanson, unpublished). This system consists of a deletion strain and a complementing plasmid that is analogous to the one for *Rb. capsulatus* that was developed by Bylina, Youvan, and coworkers.[21] Briefly, site-directed insertional mutagenesis was used to delete the chromosomal copies of structural genes for the light-harvesting II complex,[23a] as well as the light-harvesting I complex and the L and M genes of the RC (D. K. Hanson, unpublished). Mutant or wild-type RCs are expressed in trans in this deletion strain background from L and M genes borne on a derivative of broad-host-range plasmid pRK404 (tet^R).[23b] The "wild type" is $LHI^+LHII^-RC^+$.

A 7-histidine tail was also recently appended to the 3′-end of the M gene in the RC of *Rb. sphaeroides*. A plasmid bearing the His-tagged M gene was obtained from S. G. Boxer and was further engineered to make it compatible with our preexisting expression plasmid. The DH mutant was constructed in the His-tagged plasmid by site-directed mutagenesis according to the directions from a kit (Chameleon; Stratagene). Using a 63 bp mutagenic oligonucleotide, two desired codons in the M gene (M203Gly and M214Leu) were changed.[24] The presence of the desired substitutions was initially identified by the loss of a BsaI site at M203 and the loss of a SapI site at M214. The presence

of the desired mutations was confirmed by automated PCR dye terminator cycle sequencing (PE Applied Biosystems) and fluorescent sequencing instruments. The *Rb. sphaeroides* mutant was routinely grown under chemoheterotrophic conditions (semi-aerobic, dark, 34 °C) on YCC[20a] medium containing tetracycline, in the absence of selection for RC function.

RC Purification. The poly-histidine tails are on the periplasmic surface of the pigment-protein complexes from both species and associate readily with Ni- or Co-NTA (nitrilotriacetic acid) resin for rapid purification by IMAC. The basic steps in the purification of His-tagged RCs[25] were followed although we outline modifications here that facilitate the purification of the less stable *Rb. capsulatus* RCs, mutant *Rb. sphaeroides* RCs, and carotenoidless versions thereof. Briefly, cells were harvested and washed in a buffer containing 10 mM Tris, pH 7.8 and 100 mM NaCl. Cells were lysed using a sonicator and French press and cell debris was pelleted at 25 000 × *g* for 10 min. Membrane proteins (specifically RCs) were solubilized directly by the addition of 1% LDAO to the supernatant without prior isolation of the membrane fraction. Solubilization of *Rb. capsulatus* RCs proceeded at 30 °C, whereas solubilization of *Rb. sphaeroides* RCs was performed at 37 °C. The extent of solubilization was monitored judiciously via the loss of the 875 nm absorption band of the intact LHI complex. Following complete solubilization, membrane fragments were removed by ultracentrifugation at 240 000 × *g* for 1.5 h. Binding to Ni-NTA resin (Superflow; Qiagen) required a minimum of 30 min for RCs from either species. Pure protein (those with an A_{280}:A_{800} ratio of 1.8) was taken directly from the IMAC column by elution with 40 mM imidazole solution (in 0.05% LDAO buffered with 10 mM Tris, pH 7.8). To increase purity, routine anion exchange chromatography for RCs[26] was implemented. RCs were subsequently washed multiple times with 10 mM Tris, pH 7.8 and 0.05% LDAO using a spin concentrator (Ultrafree Biomax; Millipore) with a 50 kDa cutoff filter in a centrifuge operating at 2000 x *g* to dilute serially the NaCl from the RC samples and to concentrate them for TA spectroscopy. For RR studies, the *Rb. sphaeroides* DH RCs were then exchanged into 10 mM Tris (pH 8)/0.01% Triton X-100/1 mM EDTA and concentrated, and Q_A was reduced by adding a slight excess of buffered sodium dithionite solution.

The occupancy of the secondary quinone (Q_B) was found to be <2% for the samples studied here. This fact was determined by monitoring P^+Q^- charge-recombination on the millisecond-seconds time scale, using excitation with a saturating 3-ns, 532-nm flash and probing the P-band bleaching-recovery kinetics at 850 nm. It was found that >98% of the decay occurred with a time constant of 100−150 ms (depending on species) which can be ascribed to $P^+Q_A^-$ charge recombination.

The TA and RR experiments reported here were carried out on the polyhistidine-tagged DH RCs. Our previously published work on wild-type and DH RCs was performed on the nontagged proteins, purified by traditional means. As a baseline for comparisons, we have carried out extensive subpicosecond-resolved TA experiments on *Rb. capsulatus* His-tagged DH and His-tagged wild-type RCs and found no significant differences in any spectral or kinetic results for either RC compared with those reported previously on the respective nontagged proteins.

TA Measurements. The primary electron-transfer reactions were investigated on flowed samples at ∼285 K. The TA spectrometer is based on an Ar-ion pumped regeneratively amplified Ti:sapphire OPA system operated at 10 Hz. The RCs were excited with 130 fs excitation pulses at 850 or 760 nm and probed with ∼130 fs "white-light" flashes. The excitation pulses were defocused and/or attenuated such that ∼30% of the RCs were excited on a single flash. Further details of the TA apparatus, data acquisition and data analysis methods have been described elsewhere.[27]

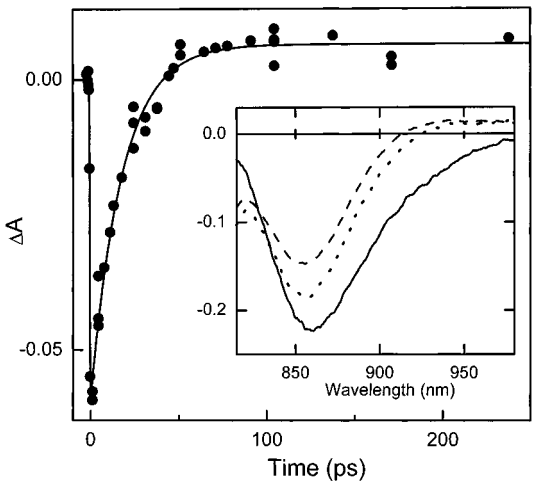

Figure 4. P* stimulated emission decay (920−930 nm) for the *Rb. sphaeroides* G(M203)D/L(M214)H mutant following excitation with a 130-fs, 750-nm excitation flash (circles). The solid line is a fit using a single exponential (plus a constant) with a time constant of 15 ps. The inset shows transient absorption difference spectra in the region of P bleaching and P* stimulated emission, acquired at 0.3 ps (solid), 50 ps (dotted), and 3 ns (dashed).

RR Measurements. The RR measurements on the *Rb. sphaeroides* DH mutant were made on optically dense (OD ∼1.0/mm at 800 nm; RC concentration ∼35 μM), snowy samples at 25 K and liquid samples at 277 K, both contained in 1 mm i.d. capillary tubes. The advantages and disadvantages of using snowy versus glassy samples have been previously discussed.[28] Temperature control was achieved by mounting the sample on a cold tip of a closed cycle refrigeration system (ADP Cryogenics, DE−202 Displex). The RR spectra were obtained using a red-optimized triple spectrograph and detection system that has been described previously.[29] Due to the large fluorescence background and the weak enhancement of the high-frequency modes of bacteriochlorins using Q_Y excitation,[28,30,31] all the RR spectra were acquired using the shifted-excitation Raman difference spectroscopic (SERDS) technique.[32,33] The application of the SERDS method to RCs has been discussed in a number of earlier publications.[18,28,31,32,34−36] Briefly, data sets acquired at two excitation wavelengths (typically 10 cm^{-1} difference) are subtracted (initial − shifted) to yield a background-free RR difference (SERDS) spectrum, which is then fit to a series of derivative-shaped functions (difference bands generated from Gaussian functions) to reconstruct the normal RR spectrum. The frequencies marked in the figures correspond to the positions of the bands used in the fits and thus, do not necessarily correspond to the peak maxima for overlapping bands. In addition, certain bands are marked that are not clearly resolved in the spectra. These bands are indicated because their inclusion noticeably improved the quality of the fits.

Results

TA Spectra and Kinetics. The presentation of the time-resolved optical data for the *Rb. sphaeroides* DH mutant in Figures 4-7 is aided by reference to the summary scheme in Figure 3B. Similarities and key differences with the analogous *Rb. capsulatus* DH mutant studied previously[11a,b] will be highlighted using representative data and the scheme in Figure 3A.

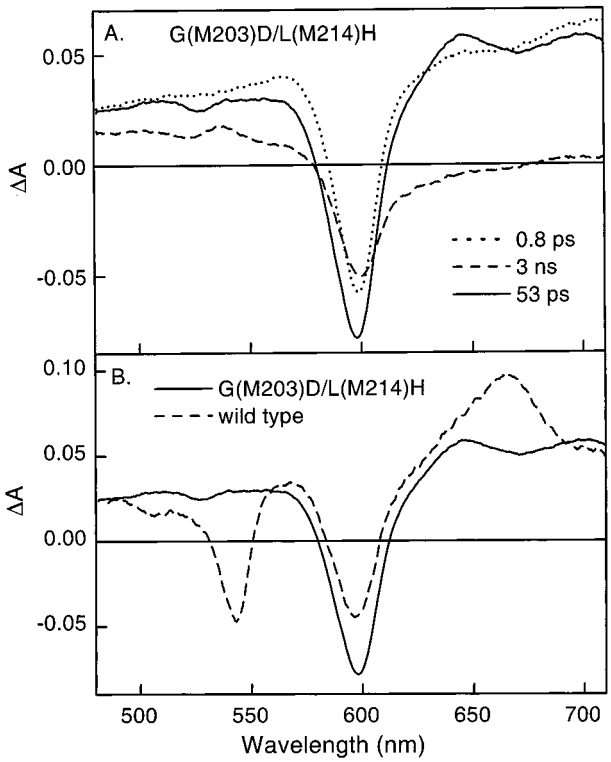

Figure 5. Transient absorption difference spectra, acquired using 130-fs, 850-nm excitation flashes, in the Q_X and anion regions for *Rb. sphaeroides* RCs: (A) G(M203)D/L(M214)H at three time delays; (B) comparison of $P^+BPh_M^-$ in G(M203)D/L(M214)H at 53 ps and $P^+BPh_L^-$ in wild type at 10 ps.

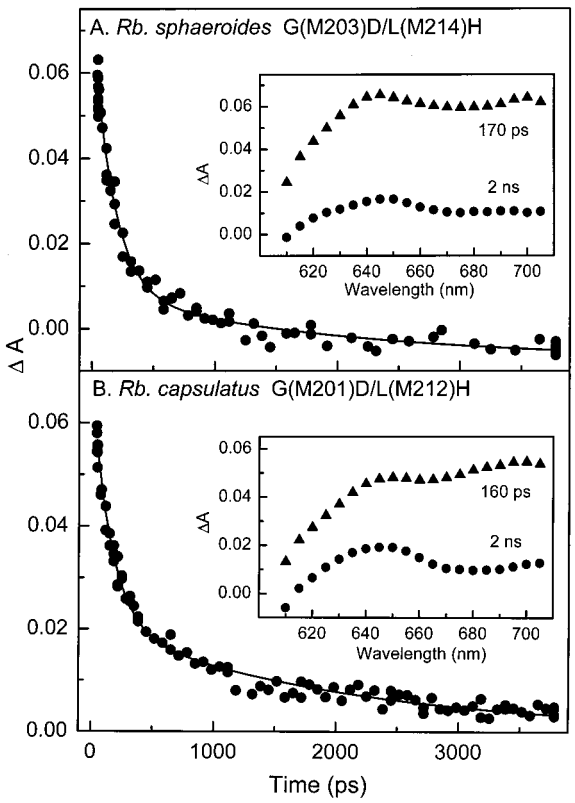

Figure 6. Anion region data for (A) *Rb. sphaeroides* G(M203)D/L(M214)H and (B) *Rb. capsulatus* G(M201)D/L(M212)H mutants. Each panel shows the time profile of the absorption changes between 640 and 650 nm acquired using 130-fs flashes at 850 nm (circles). The corresponding solid line is a fit to the sum of two exponentials plus a constant. Data acquired before and during the flash and during the P* lifetime have been omitted (see text). The inset to each panel gives the spectra of the preexponential factors of the dual exponentials fits across the entire anion absorption region. The triangles correspond to the faster (160−170 ps) component and the circles correspond to the slower (1−3 ns) component.

Excitation of the *Rb. sphaeroides* DH RC initially produces the excited primary donor, P*. The absorption difference spectrum of this state is characterized by bleaching of the 860 nm ground-state absorption band of P and concomitant stimulated emission (860−950 nm) from P* (0.3 ps spectrum in Figure 4 inset). Fitting the stimulated emission decay between 880 and 930 nm to a single-exponential plus a constant gives a P* lifetime of 15 ± 3 ps (Figure 4), which is the same as the value of 15 ± 2 ps obtained previously for the *Rb. capsulatus* DH mutant.

In wild-type RCs from both *Rb. sphaeroides* and *Rb. capsulatus*, a constant magnitude of P bleaching is observed during the P* lifetime and out to many nanoseconds after excitation, reflecting the formation of $P^+Q_A^-$ in ∼100% yield (see Figure 1). However, in the *Rb. sphaeroides* DH mutant, the amplitude of P bleaching at 3 ns is reduced ∼32% compared to its initial magnitude (Figure 4 inset). The extent of the P-bleaching decay, reflecting ground-state repopulation, is best monitored at 830−840 nm (on the blue side of the P band), where the contribution of P* stimulated emission is minimal or absent. The P-bleaching decay is clearly multiexponential at these wavelengths with a fast component of $\tau \approx 15$ ps that is readily assigned to the P* lifetime. The amplitude of this component is ∼10% of the initial P* bleaching and gives directly the yield of P* → ground state. Whether the small, additional longer-lived P-bleaching decay comprises one or two components, and the lifetimes of these components, could not be determined reliably from multiexponential fitting of the kinetic data with all parameters free.

To test/achieve consistency with kinetic data observed in the other spectral regions described below, the decay profiles between 830 and 880 nm were analyzed using three exponentials (plus a constant). In this analysis, the fast component was fixed at the P* lifetime of 15 ps (determined via decay of stimulated emission alone at 920 nm) and the slow component was set in the in the range $\tau = 1-4$ ns. This time constant, which reflects charge recombination of the M-side state $P^+BPh_M^-$, is obtained

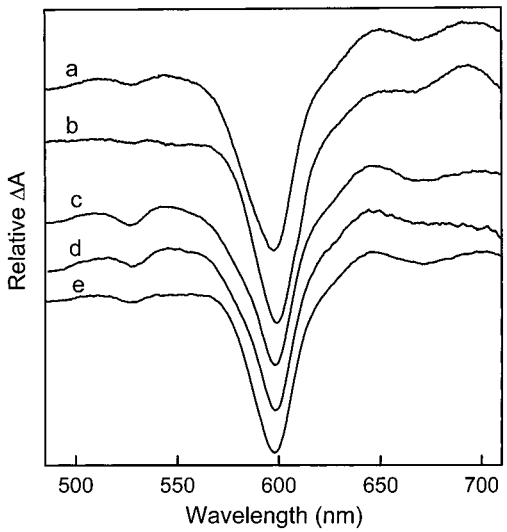

Figure 7. Transient absorption difference spectra, acquired using 130-fs, 850-nm excitation flashes, in the Q_X region for a series of RCs: (a) *Rb. capsulatus* L(M212)H, (b) *Rb. sphaeroides* L(M214)H, (c) *Rb. capsulatus* G(M201)D/L(M212)H, (d) carotenoidless *Rb. capsulatus* G(M201)D/L(M212)H, (e) *Rb. sphaeroides* G(M203)D/L(M214)H.

from data in the anion absorption region (620−720 nm) described below. The fits return a time constant of 170 ± 40 ps for the middle component that is also determined in the anion region decay kinetics. This component can be assigned to the lifetime of the L-side intermediate P^+I^- (a mixture of $P^+BChl_L^-$ and $P^+\beta^-$). The fits also give amplitudes of ∼590 and ∼15% for the ∼170 ps and 1−4 ns components, respectively, of the P-bleaching decay (ground-state recovery) kinetics, consistent with the results obtained from the spectral and kinetic data in the visible region. Thus, there is consistency between the P-bleaching recovery kinetics and the kinetics measured in the other wavelength regions, which we describe next.

Visible region TA difference spectra spanning 480 to 710 nm are shown for the *Rb. sphaeroides* DH mutant in Figure 5A. The spectrum at 0.8 ps after excitation is characteristic of P* and includes a featureless transient absorption broken by bleaching of the Q_X band of P at ∼600 nm. The spectrum at 53 ps contains a very small trough at ∼530 nm that we ascribe to bleaching of the Q_X ground-state absorption band of BPh_M arising from electron transfer in low yield to the M side to form $P^+BPh_M^-$. The 53 ps spectrum also contains a transient absorption band at ∼645 nm that we ascribe to the corresponding anion, BPh_M^-. Both of these features have been seen (but with about 2-fold larger amplitudes) and assigned similarly in the *Rb. capsulatus* DH mutant.[11a,b]

The yield of P* → $P^+BPh_M^-$ in the *Rb. sphaeroides* DH mutant was determined more accurately by comparing the BPh_M bleaching at ∼530 nm with the BPh_L bleaching at ∼545 nm for state $P^+BPh_L^-$ in the *Rb. sphaeroides* wild-type RC. Following the procedure used previously for *Rb. capsulatus*, the P* spectra (at ∼1 ps) for DH and wild-type RCs were normalized to the same initial P* concentration by a small factor (because the sample/laser conditions were not exactly the same) using the magnitude of the P bleaching at 600 nm. The same factor was then applied to the spectra corresponding to three to four P* lifetimes in each RC, namely the 53-ps spectrum in Figure 5A for the DH mutant and a spectrum at ∼10 ps for wild type. The resulting matched spectra are shown in Figure 5B. The integrated BPh_M bleaching at ∼530 nm (relative to the featureless transient absorption) in the mutant compared to the BPh_L bleaching at ∼545 nm in wild type gives a $P^+BPh_M^-$ yield of 7 ± 2% in the *Rb. sphaeroides* DH RC. This comparison assumes that the $P^+BPh_L^-$ yield is 100% in the wild-type RC and that the BPh_M and BPh_L Q_X absorption bands have the same oscillator strength. The 7% M-side yield obtained in this manner (versus 15% obtained with *Rb. capsulatus* DH RCs) is the same as that derived above from comparison of the BPh_M Q_X bleaching in the *Rb. sphaeroides* and *Rb. capsulatus* DH mutants (traces c and e of Figure 7), lending consistency to the results.

The combined 7% yield of P* → $P^+BPh_M^-$ and 10% yield of P* → ground state obtained above indicate that the majority (83%) of P* decay occurs by electron transfer to the L side (Figure 3B). This in turn implies that that 53-ps spectrum for the *Rb. sphaeroides* DH mutant in Figure 5A is dominated by the spectral characteristics of the L-side intermediate P^+I^- (a mixture of $P^+\beta^-$ and $P^+BChl_L^-$). Indeed, the strong bleaching at ∼600 nm and transient absorption between 620 and 700 nm in the 53 ps spectrum, together with other data described below, are fully consistent with this assessment. The spectrum at 3 ns in Figure 5A reflects the subsequent formation of $P^+Q_A^-$ on the L side, together with characteristics of $P^+BPh_M^-$ on the M side remaining following its partial decay.[37a]

The decay kinetics across the entire anion region (620−710 nm) are dual exponential in nature for the *Rb. sphaeroides* DH mutant (Figure 6A), due to the decay of the states formed by parallel electron transfer from P* to the L side (83%) and M side (7%) of the RC (Figure 3B). The faster component for the *Rb. sphaeroides* DH RC has $\tau = 170 \pm 40$ ps and the lifetime of the slower component is on the order of 1−4 ns.[38] The amplitude (preexponential-factor) spectra of the two components are shown in the inset to Figure 6A.[39] Generally similar dual-exponential decay kinetics and amplitude spectra have been obtained previously for the *Rb. capsulatus* DH RC (Figure 6B) and other mutants.[11] In keeping with the detailed analyses given in the previous work, the fast (∼170 ps) component for the *Rb. sphaeroides* DH RC corresponds to decay of the L-side intermediate P^+I^- (a mixture of $P^+\beta^-$ and $P^+BChl_L^-$), largely forming $P^+Q_A^-$ (∼68% yield[37b]) but with some decay to the ground state as indicated by the P-bleaching data described above. This spectral assignment is supported by the broad bands at ∼640 and ∼680 nm seen in the amplitude spectrum of the faster kinetic component in this RC (Figure 6A inset) and the *Rb. capsulatus* DH analogue (Figure 6B inset), which are characteristics consistent with BChl anions.[40] The slow (1−4 ns) component corresponds to M-side charge recombination $P^+BPh_M^-$ → ground state (Q_B is absent). This assignment is supported by the absorption band at ∼645 nm expected for the M-side anion BPh_M^- and the finding of a similar component to the P-bleaching decay.[11b,41]

The anion-region data in Figure 6 are consistent with the approximately 2-fold lower yield of electron transfer to the M branch in the *Rb. sphaeroides* DH mutant (7%) relative to the *Rb. capsulatus* analogue (15%) deduced above from the Q_X data. In particular, the *Rb. sphaeroides* mutant has a smaller amplitude of the slow component (reflecting decay of $P^+BPh_M^-$) relative to the fast component (associated with decay of the L-side intermediate). This difference can be seen from visual inspection of the kinetic traces in Figures 6A and B, and the smaller amplitude spectrum of the slow kinetic component in *Rb. sphaeroides* compared to *Rb. capsulatus*. Collectively, the visible/near-infrared data for the *Rb. sphaeroides* DH mutant at room temperature give the time constants and yields for the primary processes summarized in Figure 3B. Measurements at 77 K show differences in detail from 285 K, and are generally similar to those found previously[18] for the *Rb. capsulatus* DH mutant at 77 K.[42]

A complete study analogous to that described above for the *Rb. sphaeroides* DH mutant at 285 K was also carried out on the carotenoidless *Rb. capsulatus* DH RC. Recall from the Introduction that a motivation for studying the carotenoid(−) mutant is to eliminate the carotenoid ground state absorption and thus, the possibility of associated electrochromic shifts in the TA spectra that might result simply from L-side charge separation. Such electrochromic shifts could potentially interfere with the analysis of M-side electron transfer. Figure 8 shows that the carotenoid(−) *Rb. capsulatus* DH mutant has essentially the same ground-state absorption spectrum as the carotenoid-(+) analogue except for elimination of the carotenoid absorption, which is most pronounced between 450 and 570 nm. Traces c and d in Figure 7 demonstrate that the two RCs also have the same TA difference spectra at 53 ps in the Q_X and anion regions, most notably the identical BPh_M bleaching at ∼530 nm. Indeed all aspects of the primary events are the same in the presence or absence of the carotenoid (Figure 3A). Thus, carotenoid-associated spectral effects on the time scale of the primary processes are of no significance for assignments concerning the BPh_M bleaching at ∼530 nm and the formation and yield of $P^+BPh_M^-$ via M-side electron transfer.

RR Spectra. The high-frequency region (1375−1750 cm^{-1}) of the Q_Y-excitation (λ_{ex} = 798 nm) RR spectra of the *Rb. sphaeroides* DH RCs obtained at low (25 K) and near-ambient

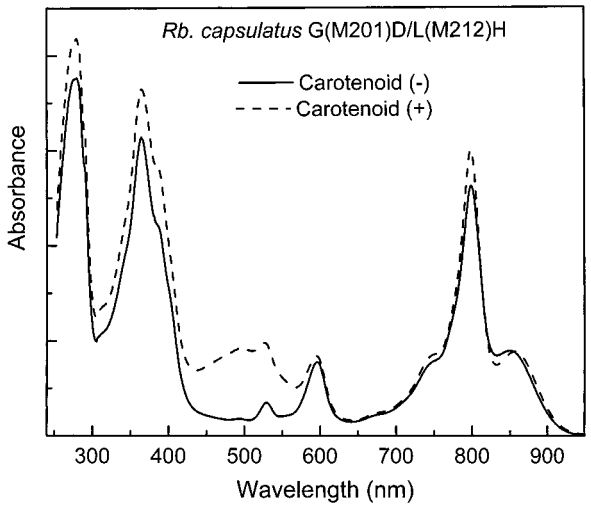

Figure 8. Ground-state absorption spectra of carotenoidless (solid) and carotenoid-containing (dashed) *Rb. capsulatus* G(M201)D/L(M212)H RCs.

(277 K) temperatures are shown in Figure 9. At each temperature, the top trace is the raw (unsmoothed) SERDS data; the second trace is the fit of the SERDS data; the third trace is the SERDS residual (observed minus fit); the bottom trace is the RR spectrum reconstructed from the SERDS data. The relatively small residuals compared with the SERDS intensities are indicative of the excellent quality of the fits. Figure 10 (left panel) compares the reconstructed RR spectra obtained for the *Rb. sphaeroides* DH RCs at 277 and 25 K with that previously reported for the *Rb. sphaeroides* wild-type RC at 25 K.[18] To facilitate further comparison, Figure 10 (right panel) shows the corresponding reconstructed RR spectra obtained previously for *Rb. capsulatus* DH and wild-type RCs.[34a] The RR spectra of wild-type RCs obtained at 277 K are not shown because these spectra for both strains are essentially identical to those obtained at 25 K, except for modest broadening of the bands at the higher temperature.[18,34a]

The RR spectra shown in Figures 9 and 10 exhibit scattering from both $BChl_L$ and $BChl_M$ because the $Q_Y(0,0)$ absorption maxima are relatively close in energy.[18,29,34a] The specific assignments for the high-frequency (1370−1750 cm^{-1}) RR bands of the two BChl cofactors in the wild-type RC[29] and a variety of genetically modified RCs[18,34a] have been previously discussed in detail and will not be reiterated herein.[43] We will largely focus on the frequencies of the key spectral features that distinguish $BChl_L$ in the DH RCs of *Rb. sphaeroides* and *Rb. capsulatus* from each other and wild-type. The frequencies of the RR bands are of particular interest because they reflect the properties of the ground electronic states of the cofactors. The RR data in Figures 9 and 10 also show that the relative intensities of certain bands differ with RC and/or temperature. The RR intensities are related to the properties of the Q_Y excited states of the chromophores (via origin shifts and/or dephasing times of certain modes) and to the excitation wavelength (resonance enhancement). It is noteworthy that previous studies have shown that the RR intensities for a cofactor can be significantly affected by altering neighboring protein residues even when the ground-state absorption features or vibrational frequencies of the cofactor are not affected to any appreciable extent.[18,36]

The key objective of the RR studies of the DH RCs was to compare how the replacement of a Gly with Asp at position M203 in *Rb. sphaeroides* affects the spectral features of the ring V C_9-keto group of $BChl_L$ relative to the analogous replacement at position M201 in *Rb. capsulatus*.[19] As a point of reference, it is important to note at the outset that spectral characteristics of the ring-V keto vibrations of $BChl_L$ and $BChl_M$ differ between wild-type RCs of the two species, at both cryogenic and near-ambient temperatures. In particular, the stretching vibrations of the C_9-keto carbonyl modes ($\nu C_9{=}O$) of $BChl_L$ and $BChl_M$ in the *Rb. capsulatus* wild-type RC both

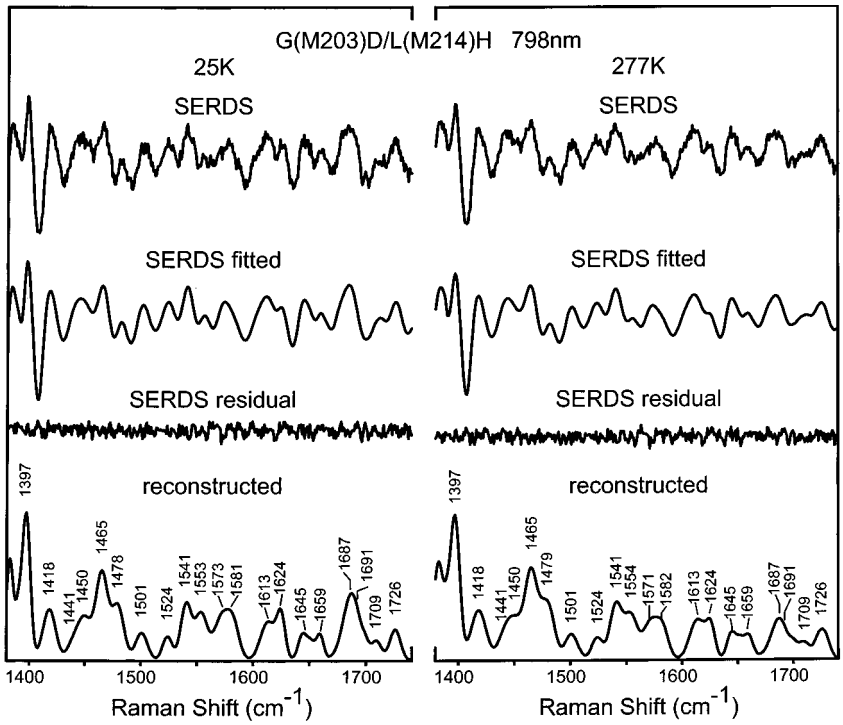

Figure 9. Q_Y-excitation (λ_{ex} = 798 nm) RR spectra of the BChls in G(M203)D/L(M214)H RCs from *Rb. sphaeroides* obtained at 25 K (left panel) and 277 K (right panel). In each panel, the top trace is the raw SERDS data, the second trace is the fit of the SERDS data, the third trace is the SERDS residual (observed minus fit), and the bottom trace is the RR spectrum reconstructed from the SERDS data.

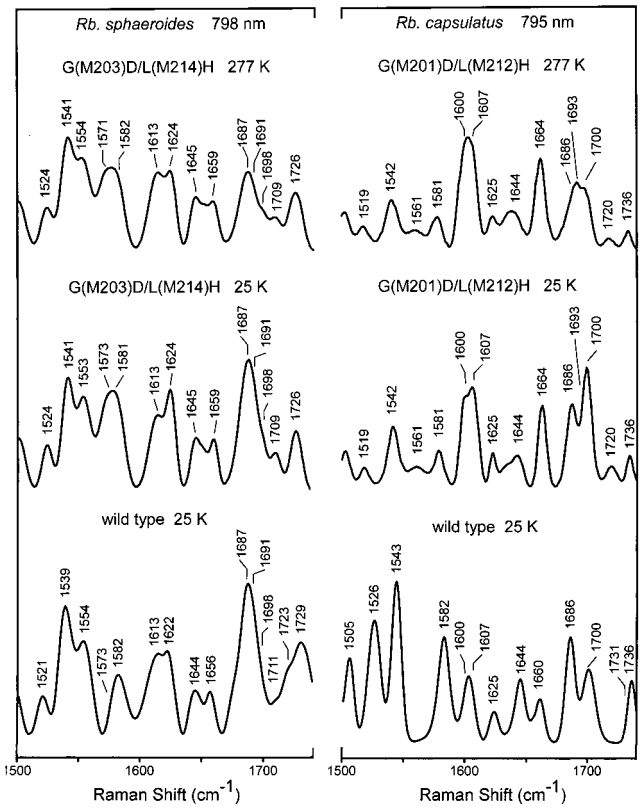

Figure 10. Comparison of the high-frequency regions of the Q_Y-excitation RR spectra of the accessory BChls in *Rb. sphaeroides* (left panel) and *Rb. capsulatus* (right panel) RCs. The top spectra are for the DH mutants, G(M203)D/L(M214)H and G(M201)D/L(M212)H, at 277 K. The middle spectra are for these same mutants at 25 K. The bottom spectra are for wild-type RCs at 25 K. The spectrum of the *Rb. sphaeroides* G(M203)D/L(M214)H mutant is the same as that shown in Figure 9 (left panel, bottom trace). The spectrum of *Rb. sphaeroides* wild-type RCs is taken from ref 34a; the spectra of *Rb. capsulatus* wild-type and G(M201)D/L(M212)H RCs are taken from ref 18.

occur at ~1686 cm^{-1} and are not resolved (Figure 10, lower right panel).[18] On the other hand, the frequencies of the νC_9=O modes of the two accessory BChls in the *Rb. sphaeroides* wild-type RC differ by ~4 cm^{-1} from one another and occur at ~1687 and ~1691 cm^{-1},[34a] although which of these features is due to $BChl_M$ and which to $BChl_L$ has not been established (Figure 10, lower left panel).[29] For both wild-type RCs, the adjacent mode centered in the vicinity of 1698−1700 cm^{-1} has been assigned as a nonfundamental vibration of the BChl macrocycle.[29]

Previous studies have shown that the replacement of Gly with Asp at M201 in the *Rb. capsulatus* DH mutant (and in the D single mutant) results in an ~7 cm^{-1} upshift of the νC_9=O mode of $BChl_L$ from 1686 to 1693 cm^{-1}.[18] Although the 1693-cm^{-1} band is not resolved in the 25 K spectrum, its presence is manifested as a shoulder and a gain in intensity of the envelope centered at ~1700 cm^{-1} at the expense of the 1686-cm^{-1} band, which in the mutant now primarily reflects the unperturbed νC_9=O mode of $BChl_M$ (Figure 10, middle versus lower right panels). The 1693-cm^{-1} band becomes even more apparent at 277 K, where a triplet of bands is observed at 1686, 1693 and 1700 cm^{-1} (Figure 10, upper right panel).[18]

In contrast, the replacement of Gly with Asp at M203 in the *Rb. sphaeroides* DH mutant engenders essentially no change in the νC_9=O vibrations from the wild-type RC and no change in the shape of the associated band contour as a function of temperature. In particular, fits of the SERDS data for the *Rb. sphaeroides* DH mutant at both 25 and 277 K reveal the presence of the two accessory-BChl νC_9=O modes at ~1687 and ~1691 cm^{-1} (plus the nonfundamental mode at ~1698 cm^{-1}), just as is observed in wild type (Figure 10, left panels).[44] Accordingly, the RR data for the DH mutant of *Rb. sphaeroides* indicate that introduction of Asp M203 has a much smaller effect on the νC_9=O vibration of $BChl_L$ than does the analogous mutation at M201 in *Rb. capsulatus*.

Discussion

The free energy gaps between the key electronic states of the RC (P*, $P^+BChl_L^-$, $P^+BPh_L^-$, and $P^+BChl_M^-$, $P^+BPh_M^-$) play critical roles in directionality of electron transfer down the L versus M sides, the mechanism(s) of the initial reactions, and the high yield of charge separation (versus charge recombination) along the L branch to form $P^+Q_A^-$. It has become increasingly clear that the free-energy position of $P^+BChl_L^-$ is a galvanizing link between these issues. The free-energy span of the L-side states (P*, $P^+BChl_L^-$, $P^+BPh_L^-$) is only ~0.25 eV, and the total span including the analogous (higher energy) M-side states is no more than ~0.5 eV (Figure 1).[11c,13b,c,10b,14,15] These close spacings are an important design issue for the native photochemistry, lead to many of the complexities observed in probing the details of the primary events, and result in effects ranging from subtle to quite dramatic when the gaps are reduced, collapsed, or even reversed in various modified RCs. The studies reported herein reveal an additional, related consequence. In particular, comparison of the primary events in the *Rb. sphaeroides* G(M203)D/L(M214)H mutant with those found previously for the *Rb. capsulatus* G(M201)D/L(M212)D analogue demonstrate that there are differences between these species in the rate constants and yields for processes on *both* the L and M sides. Differences are also seen in certain cofactor-protein interactions in the corresponding vibrational spectra. In the following, we discuss these differences for the two DH mutants and relate them to results on the simpler H mutants and to observations on wild-type RCs. We begin with a working model for how the relative free energies of the states impact the issues outlined above.

Experiments on a number of mutants demonstrate that the relative free energies of $P^+BChl_L^-$ and $P^+BChl_M^-$ with respect to P* make a substantial contribution to directionality.[11,12] These observations are consistent with the results of theoretical studies on wild-type RCs.[14] In turn, the differences in the effective rate constants for electron transfer from P* to the two branches likely derive substantially (but not solely) from relative contributions on each side of the two-step chemical-intermediate mechanism (P* → P^+BChl^- → P^+BPh^-) and the one-step process (P* → P^+BPh^-) in which P^+BChl^- serves as a superexchange mediator. In particular, because $P^+BChl_L^-$ appears to lie slightly (0.05−0.1 eV) below P*, and in order to achieve consistency between a variety of observations, a parallel combination (or hybrid) of the one-step and two-step processes must operate on the L-side.[3b,4,5a,10c,13b,14d] In contrast, electron transfer to the M side no doubt occurs exclusively by superexchange, with $P^+BChl_M^-$ above P* (by up to ~0.25 eV[14]) (Figure 1). Hence, destabilization/stabilization of $P^+BChl_L^-/P^+BChl_M^-$ via mutations modulates the associated rates/mechanisms and results in an increased M-side yield and a decreased L-side yield (see Figures 1 and 3).[11,12] Additionally, the free-energy position of $P^+BChl_L^-$ with respect to $P^+BPh_L^-$ (0.15−0.2 eV in the native RC) has surprising, dramatic consequences on the subsequent branching between charge separation and charge recombination along the L branch and thus the yield of $P^+Q_A^-$. This point becomes clear when $P^+BPh_L^-$ (or analogous states when BPh_L is replaced with another pigment) is very close (i.e., ≤ 50 meV) to $P^+BChl_L^-$.[3c,9,13] For example, in the H mutants depicted in

Figure 2, $P^+\beta^-$ is raised sufficiently with respect to $P^+BPh_L^-$ in wild type (Figure 1) that thermal/quantum mixing with $P^+BChl_L^-$ (forming P^+I^-) enhances charge recombination to the ground state and diminishes charge separation to form $P^+Q_A^-$.[9,16] Indeed, one observes an oscillation in this L-side branching ratio in a series of *Rb. capsulatus* mutants in which $P^+\beta^-$($P^+BPh_L^-$) and $P^+BChl_L^-$ are alternately destabilized.[11c]

The above-noted interrelated findings provide a framework for discussing the detailed differences in the primary reactions for *Rb. sphaeroides* and *Rb. capsulatus* RCs. The simplest kinetic scheme for the initial events has P* decaying by (1) electron transfer to the L-side with an effective[45] rate constant k_{PL}, (2) electron transfer to the M side with an effective rate constant k_{PM}, and (3) deactivation (internal conversion) to the ground state with a rate constant k_{PG}. These rate constants are obtained within this model for each RC using the measured P* lifetime and the yields of the three pathways as determined from the transient absorption data, using the relationship $k = \Phi/\tau$. Thus, for the *Rb. sphaeroides* DH mutant at 285 K, we obtain $k_{PL} = 0.83\cdot(15\text{ ps})^{-1} = (18\text{ ps})^{-1}$, $k_{PM} = 0.07\cdot(15\text{ ps})^{-1} = (210\text{ ps})^{-1}$, and $k_{PG} = 0.1\cdot(15\text{ ps})^{-1} = (150\text{ ps})^{-1}$. These values are shown in Figure 3B. The corresponding values for the *Rb. capsulatus* analogue studied previously are $k_{PL} = 0.94\cdot(15\text{ ps})^{-1} = (21\text{ ps})^{-1}$, $k_{PM} = 0.15\cdot(15\text{ ps})^{-1} = (100\text{ ps})^{-1}$, and $k_{PG} = 0.15\cdot(15\text{ ps})^{-1} = (100\text{ ps})^{-1}$, as is shown in Figure 3A. Thus, the rate of electron transfer to the M-side is about 2-fold slower in the *Rb. sphaeroides* DH RC. This difference (and perhaps a slightly faster rate of electron transfer to the L side) results in the lower yield of charge separation to the M side in the *Rb. sphaeroides* versus *Rb. capsulatus* DH mutant (7 versus 15%). [Again, this difference can be seen by comparing the respective magnitudes of BPh_M bleaching at ~530 nm in traces e and c of Figure 7.]

Consistency in these and other results can be seen by comparing the above values for the two DH mutants with rate constants for the corresponding H mutants studied previously, namely *Rb. sphaeroides* L(M214)H and *Rb. capsulatus* L(M212)H.[3b,9] In particular, the measured lifetimes and yields for the *Rb. capsulatus* H mutant give rate constants for P* decay to the two branches (Figure 2A) of $k_{PL} = 0.95\cdot(8.5\text{ ps})^{-1} = (9\text{ ps})^{-1}$ and $k_{PM} = 0.07\cdot(8.5\text{ ps})^{-1} = (120\text{ ps})^{-1}$. This M-side rate constant is in excellent agreement with the value of $(100\text{ ps})^{-1}$ derived above for the *Rb. capsulatus* DH mutant, and is in keeping with the fact that the presence of the Asp near $BChl_L$ in the DH RC should not affect the M-side process compared to the H single mutant.

For the corresponding *Rb. sphaeroides* H mutant, we previously measured a P* lifetime of 5.8 ps with no evidence of either ground-state recovery or electron transfer to the M side. Thus $k_{PL} = (5.8\text{ ps})^{-1}$. Because there was no evidence for electron transfer to the M branch, a value for k_{PM} cannot be obtained from those measurements. However, if we assume that the rate of electron transfer to the M side is approximately the same that obtained here for the *Rb. sphaeroides* DH RC, we calculate an M-side yield of (5.8 ps)/(210 ps) = 3% for the *Rb. sphaeroides* H mutant. Such a low yield of $P^+BPh_M^-$ would have been undetectable in our earlier measurements, and cannot be reliably deduced even with the higher signal-to-noise of the present measurements. This is evident in trace b in Figure 7, which shows new data with only a hint of a BPh_M bleach at ~530 nm for the *Rb. sphaeroides* H mutant, compared to the discernible bleaching seen in trace a for the *Rb. capsulatus* H mutant (7% M side yield).

Thus, the results for the DH and H mutants are consistent in showing that *Rb. sphaeroides* RCs have a lower (roughly 2-fold) overall propensity for M-side charge separation compared to *Rb. capsulatus* RCs. This difference derives from a slower rate of electron transfer to the M side in both *Rb. sphaeroides* mutants supplemented by faster L-side electron transfer compared to *Rb. capsulatus*. The latter effect is significant for the H mutants, for which $k_{PL} \approx (6\text{ ps})^{-1}$ in *Rb. sphaeroides* is about 30% faster than $(9\text{ ps})^{-1}$ for *Rb. capsulatus* (Figures 2 and 3). Indeed, a faster rate of L-side electron transfer is already present in wild-type RCs, where the P* lifetimes (reflecting ~100% electron transfer to the L side) in *Rb. sphaeroides* and *Rb. capsulatus* are 3.0 ± 0.3 and 4.3 ± 0.3 ps, respectively. Thus, the L-side rate constant $k_{PL} = (3\text{ ps})^{-1}$ for *Rb. sphaeroides* is about 30% faster than the value of $(4.3\text{ ps})^{-1}$ for *Rb. capsulatus*.

The slower rates of electron transfer to the M side for both the DH and H mutants (and by inference for wild-type) in *Rb. sphaeroides* versus *Rb. capsulatus* likely derive from specific/global effects of the protein on the (free) energy gap between $P^+BChl_M^-$ and P* in the two species, in addition to any structural effects on the relative electronic matrix elements. Calculations indicate that the free energies of the electronic states are affected by the protein as a whole, including significant contributions of residues far removed from the associated cofactors.[14a−c] Given that $P^+BChl_M^-$ no doubt lies above P* in DH, H and wild-type RCs from both species, an appropriate (free) energy shift between species would translate into reduced superexchange mixing of these states and $P^+BPh_M^-$ in *Rb. sphaeroides*.[46] Similarly, the faster L-side rates in *Rb. sphaeroides* H and wild-type (and possibly DH) RCs compared to their *Rb. capsulatus* counterparts also likely reflect differences in the relevant (free) energy gaps involving P*, $P^+BChl_L^-$, and $P^+BPh_L^-$/$P^+\beta_L^-$ within the parallel one- and two-step mechanisms (in addition to potential variations in electronic couplings).

Differences in the relative free energies of the L-side states in *Rb. sphaeroides* versus *Rb. capsulatus* are apparent not only from the initial electron-transfer processes involving decay of P* described above, but from the slower processes as well. For example, $P^+BPh_L^- \rightarrow P^+Q_A^-$ electron transfer is slower in *Rb. sphaeroides* versus *Rb. capsulatus* wild-type RCs, namely, $k_{IQ} \approx (210\text{ ps})^{-1}$ versus $(160\text{ ps})^{-1}$ (Figure 1). Additionally, the H mutants of the two species have different branching ratios for decay of the effective L-side intermediate P^+I^- via charge separation (to form to $P^+Q_A^-$) or charge recombination (to give the ground state) (Figure 2). These findings and the associated temperature dependences of the branching ratio suggest that $P^+BChl_L^-$ lies below $P^+\beta_L^-$ in the *Rb. sphaeroides* H mutant whereas the two states are essentially degenerate in the *Rb. capsulatus* analogue.[3b] Thus, the two states apparently give different weighting to the character of P^+I^- in the respective H mutants. This difference may also be manifested in the difference in the shapes of the anion-region spectra (620−720 nm) and in the exact position and width of the absorbance decrease at ~600 nm in traces a and b of Figure 7. Differences in the branching ratio for decay of the L-side intermediate are also seen in the DH mutants from the two species and again, likely originate from different contributions of $P^+BChl_L^-$ and $P^+\beta_L^-$ (Figure 3).

What are the origins of the differences between the electron-transfer rates in analogous *Rb. sphaeroides* and *Rb. capsulatus* RCs (Figures 1-3)? As noted above, these could be due in part to small architectural differences (distances, orientations, etc) and associated electronic matrix elements. However, it is likely that a significant contribution comes from differences in the (free) energy gaps between the relevant states in the two species. Because the total span between P* and $P^+BChl_L^-$ and $P^+BPh_L^-$ is only ~0.25 eV in wild type and less in many mutants, differences in free energies of tens of meV could result in the rates being dependent on species and specific RC. As a point

of reference, free-energy variations of this magnitude associated with structural/energetic population distributions of proteins in a given RC sample are thought to contribute to the observed photodynamic properties.[5a,b,6,15,47] Thus, it is reasonable that small differences in free-energy gaps between states in *Rb. capsulatus* and *Rb. sphaeroides* may give rise to observable differences in electron-transfer rates. The differences in P* electron transfer to the two branches may be due in part to a slightly (~0.03 eV) lower energy of P* *Rb. sphaeroides*, as indicated by the typical positions of the respective P bands in the room-temperature ground-state absorption spectra of the isolated RCs (~865 versus ~850 nm). However, it is unlikely that this is the sole contributing factor for the differences in the P* decay channels;[48] the relative positions of the charge-separated states must also come into play. Indeed, variations in the energy gaps involving $P^+BChl_L^-$ and $P^+BPh_L^-/P^+\beta_L^-$ must underlie differences in the nature and decay rates of the L-side intermediate between analogous RCs (wild type, H, DH), as these gaps are independent of the P* energy or the P/P^+ potential. Furthermore, the RR data indicate that there are differences between the interactions of $BChl_L$ (and perhaps other cofactors) with the protein environment in *Rb. sphaeroides* versus *Rb. capsulatus*, both for DH and wild-type RCs. These interactions and others not seen in the vibrational spectra may contribute to differences in the (free) energies of the charge-separated states with species.

Conclusion

The picture that emerges from the studies reported herein is that it is quite reasonable that there are differences in rate constants for individual electron-transfer steps in analogous RCs from different species, such as *Rb. sphaeroides* and *Rb. capsulatus* (as is observed for the DH, H, and wild-type RCs). It also seems reasonable that these differences are due in part to species-dependent small (tens of meV) variations in the (free) energy gaps between states, perhaps with contributions of the electronic matrix elements. The effects would appear to be another consequence of the rather modest free-energy gaps in the wild-type RC. The small differences between species have observable effects on the lifetimes of the states (e.g., P* and $P^+BPh_L^-$), but insignificant effects on the yields of charge separation to the L side and farther along this branch in the native system. However, when the modest free-energy gaps are diminished or the ordering of the states is reversed as a consequence of genetic manipulation, the intrinsic small differences in energetics between species can have dramatic consequences. An additional specific conclusion from the work described herein is that *Rb. sphaeroides* RCs have both a reduced propensity for M-side transfer and a greater tendency for L-side transfer, making it more difficult to elicit charge separation down the normally inactive branch compared to the *Rb. capsulatus* analogues.

Acknowledgment. This work was supported by Grant MCB-0077187 (C.K. and D.H.) from the National Science Foundation, Grant GM-39781 (D.F.B.) from the National Institute of General Medical Sciences. P.D.L., A.N.H., and D.K.H. were supported by the United States Department of Energy, Office of Biological and Environmental Research, under contract W-31-109-ENG-38.

References and Notes

(1) (a) Ermler, U.; Fritzsch, G., Buchanan, S.; Michel, H. *Structure* **1994**, *2*, 925−936. (b) Deisenhofer, J.; Epp, O., Sinning, I.; Michel, H. *J. Mol. Biol.* **1995**, *246*, 429−457. (c) Yeates, T. O.; Komiya, H.; Chirino, A.; Rees, D. C.; Allen, J. P.; Feher, G. *Proc. Natl. Acad. Sci. U.S.A.* **1988**, *85*, 7993−7997. (d) El-Kabbani, O.; Chang, C.-H.; Tiede, D.; Norris, J.; Schiffer, M. *Biochemistry* **1991**, *30*, 5361−5369. (e) Komia, H.; Yeates, T. O.; Rees, D. C.; Allen, J. P.; Feher, G. *Proc. Natl. Acad. Sci. U.S.A.* **1988**, *85*, 9012−9016.

(2) (a) Deisenhofer, J.; Norris, J. R., Eds. *The Photosynthetic Reaction Center*, Academic: San Diego, 1993; Vol. II; (b) Blankenship, R. E.; Madigan, M. T.; Bauer, C. E., Eds. *Anoxygenic Photosynthetic Bacteria*; Kluwer Academic Publishers: Dordrect, The Netherlands, 1995. (c) Michel-Beyerle, M. E., Ed. *The Reaction Center of Photosynthetic Bacteria*; Springer, Berlin-Heidelberg, 1996.

(3) (a) Bylina, E. J.; Kirmaier, C.; McDowell, L.; Holten, D.; Youvan, D. C. *Nature* **1988**, *336*, 182−184. (b) Heller, B. A.; Holten, D.; Kirmaier, C. *Biochemistry* **1996**, *35*, 15 418−15 427. (c) Laporte, L. L.; Palaniappan, V.; Davis, D. G.; Kirmaier, C.; Schenck, C. C.; Holten, D.; Bocian, D. F. *J. Phys. Chem.* **1996**, *44*, 17 696−17 707.

(4) Nagarajan, V.; Parson, W. W.; Davis, D.; Schenck, C. C., *Biochemistry* **1993**, *32*, 12 324−12 336.

(5) (a) Jia, Y.; DiMagno, T. M.; Chan, C. K.; Wang, Z.; Du, M.; Hanson, D. K.; Schiffer, M.; Norris, J. R.; Fleming, G. R.; Popov, M. S. *J. Phys. Chem.* **1993**, *97*, 13 180−13 191. (b) Laible, P. D.; Greenfield, S. R.; Wasielewski, M. R.; Hanson, D. K.; Pearlstein, R. M. *Biochemistry* **1997**, *97*, 88 677−88 685.

(6) Hamm, P.; Gray, K. A.; Oesterhelt, D.; Feick, R.; Scheer, H.; Zinth, W. *Biochim. Biophys.* Acta **1993**, *1142*, 99−105.

(7) Streltsov, A. M.; Vulto, S. I. E.; Shkurapatov, A. Ya.; Hoff, A. J.; Aartsma, T. J.; Shuvalov, V. A. *J. Phys. Chem. B.* **1998**, *102*, 7293−7298.

(8) (a) Zhou, H.; Boxer, S. G. *J. Phys. Chem. B.* **1998**, *102*, 9139−9147. (b) King, B. A.; McAnaney, T. B.; deWinter, A.; Boxer, S. G. *J. Phys. Chem. B.* **2001**, *105*, 1856−1862.

(9) (a) Kirmaier, C.; Gaul, D.; DeBey, R.; Holten, D.; Schenck, C. C. *Science* **1991**, *251*, 922−927. (b) Kirmaier, C.; Laporte, L.; Schenck, C. C.; Holten, D. *J. Phys. Chem.* **1995**, *99*, 8910−8917.

(10) (a) Williams, J. C.; Alden, R. H.; Murchison, H. A.; Peloquin, J. M.; Woodbury, N. W.; Allen, J.P. *Biochemistry* **1992**, *31*, 11 029−11 037. (b) Peloquin, J. M.; Williams, J. C.; Lin, X.; Alden, R. G.; Taguchi, A. K. W.; Allen, J. P.; Woodbury, N. W. *Biochemistry* **1994**, *33*, 8089−8100. (c) Woodbury, N. W.; Peloquin, J. M.; Alden, R. G.; Lin, X.; Lin, S.; Taguchi, A. K. W.; Williams, J. C.; Allen, J. P. *Biochemistry* **1994**, *33*, 8101−8112.

(11) (a) Heller, B. A.; Holten, D.; Kirmaier, C. *Science* **1995**, *269*, 940−945. (b) Kirmaier, C.; Weems, D.; Holten, D. *Biochemistry* **1999**, *38*, 11 516−11 530. (c) Roberts, J. A.; Holten, D.; Kirmaier, C. *J. Phys. Chem. B.* **2001**, *105*, 5575−5584.

(12) (a) Katilius, E.; Turanchik, T.; Lin, S.; Taguchi, A. K. W.; Woodbury, N. W. *J. Phys. Chem. B.* **1999**, *103*, 7386−7389. (b) Lin, S.; Xiao, W.; Eastman, J. E.; Taguchi, A. K. W.; Woodbury, N. W. *Biochemistry* **1996**, *35*, 3187−3196.

(13) RCs in which BPh_L is replaced with another pigment such as plant pheophytin exhibit photochemical behavior different from wild-type and analogous to the H RCs.[9] (a) Shkurapotov, A. Y.; Shuvalov, V. A. *FEBS Lett.* **1993**, *322*, 168−172. (b) Schmidt, S.; Arlt, T.; Hamm, P.; Huber, H.; Nagele, T.; Wachtveitl, J.; Meyer, H.; Scheer, H.; Zinth, W. *Chem. Phys. Lett.* **1994**, *223*, 116−120. (c) Kennis, J. T. M.; Shkuropatov, A. Y.; van Stokkum, I. H. M.; Gast, P.; Hoff, A. J.; Shuvalov, V. A.; Aartsma, T. J. *Biochemistry* **1997**, *36*, 16 231−16 238.

(14) (a) Parson, W. W.; Chu, Z.-T.; Warshel, A. *Biochim. Biophys Acta* **1990**, *1017*, 251−272. (b) Alden, R. G.; Parson, W. W.; Chu, Z. T.; Warshel, A. *J. Phys. Chem.* **1996**, *100*, 16 761−16 770. (c) Gunner, M. R.; Nicholls, A.; Honig, B. *J. Phys. Chem.* **1996**, *100*, 4277−4291. (d) Bixon, M.; Jortner, J.; Michel-Beyerle, M. E. *Chem. Phys*. **1995**, 197, 389−404. (e) Pudlak, M.; Pincak, R. *Chem. Phys. Lett.* **2001**, *342*, 587−592.

(15) (a) Gunner, M. in *Current Top. Bioenergetics* **1991**, *16*, 319. (b) Goldstein, R. A.; Boxer, S. G. *Biochim. Biophys. Acta* **1989**, *977*, 70−77. (c) Hartwich, G.; Lossau, H.; Michel-Beyerle, M. E.; Ogrodnik, A. *J. Phys. Chem. B.* **1998**, *102*, 3815−3820.

(16) (a) Charge recombination of the L-side transient intermediate increases with increasing contribution of $P^+BChl_L^-$ in the simplest terms because of the closer hole-electron separation compared to $P^+BPh_L^-$ (or $P^+\beta_L^-$). Similarly, electron transfer to Q_A is slowed because of the larger distance involved. (b) Such branched photochemistry is observed in RCs in which BPh_L is replaced by a BChl (β) via mutagenesis,[9, 11a] is replaced by another pigment via chemical treatment[13] or has a Asp residue placed nearby.[3b]

(17) The G(M201)D mutations in *Rb. capsulatus* and the corresponding G(M203)D mutation in *Rb. sphaeroides* do not affect the redox potential or optical characteristics of P, but only the optical and vibrational properties of $BChl_L$.[10a,11a] The Asp significantly raises the free energy of state $P^+BChl_L^-$ (probably 100−150 meV), as deduced by effects on electron transfer in a number of *Rb. capsulatus* RCs containing the G(M201)D mutation.[11] The vibrational data indicate that D is not hydrogen bonded to the ring V keto group of $BChl_L$, and may be ionized, at least at room temperature.[18] An increase in the free energy of $P^+BChl_L^-$ is consistent with this ionization state of the Asp, but also may accounted for by dipole-

dipole or other effects if the Asp is protonated, as long as the effects significantly destabilize $P^+BChl_L^-$.[11a] The proposed displacement[17b] of a nearby water molecule found in the wild-type *Rb. sphaeroides*[1a] structure could make such a contribution. Hydrogen-bonding involving $BChl_L$ with such water molecules should not contribute significantly because such bonding is not commensurate with the vibrational data on wt RCs or the G(M201)D mutant (at least when P is neutral).[17c−f,18,29,34a] (b) Fyfe, P. K.; Ridge, J. P.; McAuley, K. E.; Cogdell, R. J.; Isaacs, N. W.; Jones, M. R *Biochemistry* **2000**, *39*, 5953−5960. (c) Lutz, M.; Robert, B. In *Biological Applications or Raman Spectroscopy*; Spiro, T. G., Ed.; Wiley: New York, 1988; Vol 3, pp 347−411. (d) Lutz, M.; Mantele, W. In *Chlorophylls*; Scheer, H., Ed.; CRC Press: Boca Raton, FL, 1991; pp 855−902. (c) Lutz, M. *Biospectroscopy* **1995**, *1*, 313−327. (f) Palanniappan, V.; Bocian, D. F. *J. Am. Chem. Soc.* **1995**, *117*, 3647−3648.

(18) Czarnecki, K.; Kirmaier, C.; Holten, D.; Bocian, D. F. *J. Phys. Chem. A.* **1999**, *103*, 2235−2246.

(19) Because of the different lengths of the M chains, residues M214Leu and M212Leu are structurally analogous in the RCs of *Rb. sphaeroides* and *Rb. capsulatus*, respectively. Likewise, residues M203Gly and M201Gly are analogous.

(20) (a) Taguchi, A. K. W.; Stocker, J. W.; Alden, R. G.; Causgrove, T. P.; Peloquin, J. M.; Boxer, S. G.; Woodbury, N. W. *Biochemistry* **1992**, *31*, 10 345−10 355. (b) Lin, X.; Murchison, H. A.; Nagarajan, V.; Parson, W. W.; Allen, J. P.; Williams, J. C. *Biochemistry* **1994**, *33*, 10 265−10 269. (c) Xiao, W.; Lin S.; Taguchi, A. K. W.; Woodbury, N. W. *Biochemistry*, **1994**, *33*, 8313−8322.

(21) (a) Youvan, D. C.; Ismail, S.; Bylina, E. J. *Gene*, **1985**, *33*, 19−30. (b) Bylina, E. J.; Ismail, S.; Youvan, D. C. *Plasmid* **1986**, *16*, 175−181. (c) Bylina, E. J.; Jovine, R. V. M.; Youvan, D. C. *Bio/Technology*, **1989**, *7*, 69−74. (d) Kolaczkowski, S. V.; Bylina, E. J.; Youvan, D. C.; Norris, J. R. In *Molecular Biology of Membrane-Bound Complexes in Phototrophic Bacteria*; Drews, G., Ed; Plenum: New York, 1990; pp 305−312.

(22) Laible, P. D.; Chynwat, V.; Thurnauer, M. C.; Schiffer, M.; Hanson, D. K.; Frank, H. A. *Biophys. J.* **1998**, *74*, 2623−2637.

(23) (a) Lee, J. K.; Kiley, P. J.; Kaplan, S. *J. Bacteriol.* **1989**, *171*, 391−3405. (b) Ditta, G.; Schmidhauser, T.; Yakobsen, E.; Lu, P.; Liang, X.-W.; Finlay, D. R.; Guiney, D.; Helinski, D. R. *Plasmid* **1985**, *13*, 149−153.

(24) (a) Care was taken to substitute codons preferred by *Rhodobacter* (e.g., CAC was used for M214His instead of CAT); however, GAT was used to encode Asp at M203 because it only required a single mismatch from the native Gly codon GGT and because it was the codon used to construct the analogous M201D substitution in the DH mutant of *Rb. capsulatus*.[11a] Although we note that GAT is a relatively rarely used Asp codon in the *Rhodobacter* photosynthetic gene cluster,[24b] its presence does not appear to affect the yield of recombinant protein. (b) Williams, J. C.; Taguchi, A. K. W. In: *Anoxygenic Photosynthetic Bacteria*; Blankenship, R. E., Madigan, M. T., Bauer, C. E., Eds; Kluwer Academic Publishers: Dordrecht, The Netherlands, 1995; pp 1029−1065.

(25) Goldsmith, J. O.; Boxer, S. G. *Biochim. Biophys. Acta* **1996**, *1276*, 171−175.

(26) Tiede, D. M.; Vazquez, J.; Cordova, J.; Marone, P. A. *Biochemistry* **1996**, *35*, 10 763−10 775.

(27) (a) Kirmaier, C.; Holten, D. *Biochemistry* **1991**, *30*, 609−613. (b) Yang, S. I.; Li, J.; Cho, H. S.; Kim, D.; Bocian, D. F.; Holten, D.; Lindsey, J. S. *J. Mater. Chem.* **2000**, *10*, 283−296.

(28) Palaniappan, V.; Schenck, C. C.; Bocian, D. F. *J. Phys. Chem.* **1995**, *99*, 17 049−17 058.

(29) Palaniappan, V.; Martin, P. C.; Chynwat, V.; Frank, H. A.; Bocian, D. F. *J. Am. Chem. Soc.* **1993**, *115*, 12 035−12 049.

(30) Diers, J. R.; Bocian, D. F. *J. Am. Chem. Soc.* **1995**, *117*, 6629−6630.

(31) Cherepy, J. M.; Shreve, A. P.; Moore, L. J.; Boxer, S. G.; Mathies, R. A. *Biochemistry* **1997**, *36*, 8559−8566.

(32) Cherepy, N. J.; Shreve, A. P.; Moore, L. J.; Franzen, S.; Boxer, S. G.; Mathies, R. A. *J. Phys. Chem.* **1994**, *98*, 6023−6029.

(33) Shreve, A. P.; Cherepy, N. J.; Mathies, R. A. *Appl. Spectrosc.* **1992**, *46*, 707−711.

(34) (a) Czarnecki, K.; Schenck, C. C.; Bocian, D. F. *Biochemistry* **1997**, *36*, 14 697−14 704. (b) Czarnecki, K.; Diers, J. R.**;** Chynwat, V.; Erickson, J. P.; Frank, H. A.; Bocian, D. F. *J. Am. Chem. Soc.* **1997**, *119*, 415−426. (c) Czarnecki, K.; Chynwat, V.; Erickson, J. P.; Frank, H. A.; Bocian, D. F. *J. Am. Chem. Soc.* **1997**, *119*, 2594−2595.

(35) (d) Cherepy, N. J.; Holzwarth, A.; Mathies, R. A. *Biochemistry* **1995**, *34*, 5288−5293. (d) Cherepy, N. J.; Shreve, A. P.; Moore, L. J.; Boxer, S. G.; Mathies, R. A. *J. Phys. Chem. B* **1997**, *101*, 3250−3260.

(36) Cua, A.; Kirmaier, C.; Holten, D.; Bocian, D. F. *Biochemistry* **1998**, *37*, 6394−6401.

(37) (a) There is a more apparent shift of the BPh absorption upon $P^+Q_A^-$ formation in *Rb. sphaeroides* than *Rb. capsulatus*. (b) The $P^+Q_A^-$ yield for each RC is based on P-bleaching amplitude at 3 ns compared to P* at 0.3 ps. The yield may be slightly (up to ∼5%) smaller than the value obtained in this manner, depending on the decay time (1−4 ns) of the M-side intermediate $P^+BPh_M^-$ and thus its contribution at 3 ns, as noted previously for other mutants.[11b,c]

(38) Because the data extend to only 3.8 ns and this at best is about four 1/e times of the slower component, the error in the associated time constant for the longer-lived component in the anion-region and P-bleaching decay is much larger than indicated by simple best fits (1.0 ± 0.4 ns and 1.2 ± 0.4 ns, respectively). For example, in the anion region, holding the slow component fixed at 1.5, 2.0, 2.5, or 3.0 ns gives visually good fits to the anion region data in Figure 6, with the value of the faster time constant only marginally changed. The use of time constants longer than about 4 ns for the slow component gives poorer fits and unreasonable spectra at the asymptote of the decay. These considerations suggest that the time constant of the slower component is likely in the 1−4 ns range. This behavior parallels that previously observed for the DH and KDH mutants.[11a,b]

(39) (a) The amplitude spectra in Figure 6 (insets) were generated from fits in which the value of the longer component was held fixed at 2.5 ns. Varying this time constant between 1.0 and 3.5 ns does not appreciably affect the derived spectra. (b) The amplitude spectrum of the slower component also has a second weak feature near 700 nm that is also present in $P^+Q_A^-$ spectra and that can be assigned to P^+.[11b, c]

(40) Fajer, J., Borg, D. C.; Forman, A., Dolphin, D.; Felton, R. H. *J. Am. Chem. Soc.* **1973**, *95*, 42 739.

(41) BPh_M^- has been produced in steady-state photochemical trapping experiments: Robert, B.; Tiede, D. M.; Lutz, M. *FEBS Lett.* **1985**, *183*, 326−330. Kellogg, E. C.; Kolaczkowski, S.; Wasiewlewski, M. R.; Tiede, D. M. *Photosynth. Res.* **1989**, *22*, 47−59. Gray, K. A.; Wachtveitl, J.; Oesterhelt, D. *Eur. J. Biochem* **1992**, *207*, 723−731. The exact position of the BPh_M^- absorption is not the same in the steady-state experiments in which this anion is trapped and in the transient experiments in which state $P^+BPh_M^-$ is formed. In the latter case, the difference spectra contain contributions from P^+ (see ref 39b) as well as bleaching and electroctrochromic shifts involving the Q-bands (∼600 nm) of P, $BChl_L$, $BChl_M$, and BPh_L/β (see ref 9b).

(42) A notable difference in the *Rb. sphaeroides* DH RC at 77 K compared to 285 K is the finding that the P* stimulated emission decay is dual exponential. The fast component has a lifetime (20 ± 10 ps) that is comparable to that found at 285 K (15 ± 3 ps). The slower component has a time constant of 350 ± 150 ps, and likely reflects thermal repopulation of P* from L-side intermediate P^+I^- (a mixture of $P^+\beta^-$ and $P^+BChl_L^-$). Such delayed P* stimulated emission was also found previously for the analogous *Rb. capsulatus* DH mutant at 77 K (lifetime 470 ± 80) ps.[18]

(43) The vibrations enhanced with Q_Y excitation include the stretching modes of the C_{10a}-carbomethoxy (1725−1755 cm^{-1}) and C_9-keto (1685−1705 cm^{-1}) carbonyl groups (both on ring V), the C_{2a}-acetyl (1650−1680 cm^{-1}) carbonyl group (on ring II), as well as stretching modes of the C_aC_m and unsaturated C_bC_b bonds (1600−1640 cm^{-1}).[22b,31c−f] The remaining stretching modes of the C_aC_m bonds as well as those of the C_aC_b and C_aN bonds occur at lower frequencies (1300−1600 cm^{-1}; not shown).[17c−f,29]

(44) We cannot rule out small shifts (a few wavenumbers) in the *Rb. sphaeroides* DH mutant relative to wild type because that equally good fits to the SERDS data can be obtained by shifting either of the 1687- or 1691-cm^{-1} bands by a small amount.

(45) An effective rate constant for electron transfer to each branch is used in the simple kinetic model because one- and two-step mechanisms are operative in parallel to an extent depending on the branch and the RC.

(46) In the simplest view, this would imply that $P^+BChl_M^-$ is slightly farther above P* than in *Rb. capsulatus*. However, this rigorously may not be the case because the relevant energy denominator depends on the relationships of the potential energy surfaces of all three states, which does not correspond directly to the equilibrium (free) energy gap between $P^+BChl_M^-$ and P*. Note also that the energy (not free energy) gap is relevant for mixing the states within the superexchange formalism (assuming the typical perturbation-theory analysis). The free energy gaps are of principal importance for the two-step mechanism, which operates in parallel with the one-step process on the L side (e.g., in wild type) and potentially on the M side if $P^+BChl_M^-$ drops below P* as a result of genetic manipulation of the RC.

(47) (a) Kirmaier, C.; Holten, D. *Proc. Natl. Acad. Sci. U.S.A.* **1990**, *97*, 3522−3556. (b) Volk, M., Aumeier, G., Langenbacher, T., Feick, R., Ogrodnik, A., Michel-Beyerle, M. E. *J. Phys. Chem. B.* **1998**, *102*, 735−751.

(48) The absorption band of P can be shifted from ∼830 to ∼850 nm (corresponding to an ∼0.03 eV difference in the P* energy) by altering a series of nearby amino acid residues, with no measurable change in the rate constant for electron transfer to the L branch; Eastman, J. E.; Taguchi, A. K. W.; Lin, S.; Jackson, J. A.; Woodbury, N. W. *Biochemistry* **2000**, *39*, 14787−14789.